Defect modes in otherwise perfect photonic crystals and photonic crystal fibers

Martijn de Sterke[a], Lindsay Botten[b], Ross McPhedran[a], Stewart Wilcox[a], Boris Kuhlmey[a] and David Fussell[a]

[a]School of Physics and Centre for Ultrahigh-bandwidth Devices for Optical Systems (CUDOS), University of Sydney, Sydney 2006, Australia.

[b]School of Mathematical Sciences and Centre for Ultrahigh-bandwidth Devices for Optical Systems (CUDOS), University of Technology Sydney, Sydney 2007, Australia.

ABSTRACT

Many of the applications of photonic crystals and photonic crystal fibers require the periodic structure to have some type of defect. In photonic crystal fibers a point defect defines the fiber core, whereas in photonic crystals a line defect acts as a waveguide, and point defects act as cavities. The modeling of these defects usually either makes use of periodic boundary conditions, by which the defect is replicated periodically, or models a photonic crystal of finite extent. However, some applications, for example the cut-off behavior of a defect mode where the field extends very widely, require methods that can model a defect in an otherwise infinite and perfectly periodic structure. Here we present such a method. It combines the method of fictitious sources with averaging over the Brillouin zone, and we apply it to study the long-wavelength behavior of the fundamental mode of photonic crystal fibers.

Keywords: Photonic crystals, photonic crystal fibers, microstructured optical fibers, defect modes. Bloch modes, multipole methods.

1. INTRODUCTION

While photonic band gaps—frequency ranges in which the propagation of light is suppressed through Bragg reflection—form the foundation of the technological potential of many photonic crystal structures, it is the introduction of defects into an otherwise periodic medium (e.g., waveguides, cavities etc) that allows this potential to be realized. The introduction of defects into photonic crystal structures gives rise to defect modes, the frequencies of which lie in the band gap of the surrounding PC, and thus are localized.

To date, the modeling of defect modes in imperfect periodic structures has been undertaken using techniques that assume a finite structure—either explicitly or implicitly, as in supercell methods which periodically replicate a finite structure. While such methods work well for strongly confined modes, difficulties arise when the mode becomes extended. The computational requirements of modeling a sufficiently large structure can then become overwhelming and lead to inaccurate results if the mode is poorly confined.

To handle such problems, as typically arise in studying a mode near cutoff [1,2,3], we have developed an exact theory for computing defect modes in a *genuinely infinite* 2D lattice, and we apply it here to study the long-wavelength behavior of microstructured optical fibers (MOF). Not only does the theory handle MOFs with an infinite cladding, but also it is computationally more efficient than other techniques when the size of the structure becomes large. This method thus allows for calculations similar to those for conventional fibers, which, because of their relatively simple geometry, are also modeled with infinite claddings. Though the cladding in these fibers is actually of course finite, it is nonetheless sufficiently large for possible modeling errors to be completely negligible. One might expect that with further improvements in technology a similar situation will occur with MOFs: namely that their cladding becomes so large that confinement losses and other finite cladding effects are negligible, and therefore for MOFs to be well-modeled as having infinite cladding.

Photonic Crystals and Fibers, edited by Waclaw Urbanczyk, Bozena Jaskorzynska, Philip St. J. Russell, Proc. of SPIE Vol. 5950, 595002, (2005) · 0277-786X/05/$15 · doi: 10.1117/12.620657

In Sec. 2 we develop the *fictitious source superposition method* (FSS) [4] for a simple (single cylinder) defect and plane incidence, noting that the theory extends naturally to arbitrary incidence and general defects. Here, we focus the three main conceptual ideas that lie at its heart. The immediate motivation for the development of this method w the need to resolve the issue of a possible cutoff of the fundamental mode of index-guided MOFs. Previous work some of us [2], suggested that this mode does have a cutoff at long wavelengths. However, this conclusion was bas on the extrapolation of results for MOFs with large but finite cladding. In Sec. 3 then, we apply the FSS method study this issue, making use of the FSS's capability to model structures with genuinely infinite cladding. This is a d manding problem, for which the FSS is eminently well suited, since the mode field becomes very large even at wav lengths that are not much larger than the spacing of the holes in the MOF cladding. Finally, in Sec. 4 we discuss o work and draw some conclusions.

2. THEORY AND IMPLEMENTATION

2.1. Nomenclature and definitions

The aim of this method is to model the modes of the structure shown in Fig. 1, comprising cylinders of radius a arranged in a regular lattice with lattice constant d, interlayer spacing h and with lattice vectors $\mathbf{e}_1$ and $\mathbf{e}_2$. The central cylinder is either removed or altered (e.g., by changing its radius or refractive index) to form a defect.

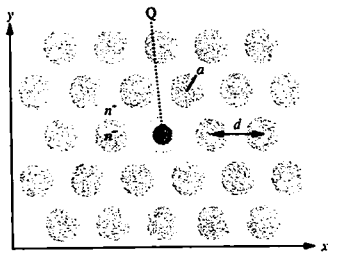

Fig. 1. Schematic of the geometry with cylinders of radius a and refractive index n_i in a background of refractive index n_e. The defect is formed by removing the central cylinder, or by changing its radius, refractive index or shape.

While ultimately we will be solving problems in 3D, for convenience and simplicity we will outline the method in 2D, explaining the salient differences and generalizations as we proceed. In 2D, we begin by considering the solution in either of the two fundamental polarizations, respectively $E_{\|}$ and $H_{\|}$, in which the problem is solved in terms of scalar fields $V(\mathbf{r}) = E_z$ and $V(\mathbf{r}) = H_z$, representing the components of the electric and magnetic field vectors parallel to the axes of the cylinders. In either case, V satisfies a Helmholtz equation $(\nabla^2 + k_j^2)V = 0$, where k_j denotes the wavenumber in the particular medium.

In the exterior vicinity of each cylinder centred at $\mathbf{c}_j$, we represent the fields in terms of a multipole expansions [5,6] involving cylindrical harmonic functions,

$$V_e(\mathbf{r}+\mathbf{c}^j) = \sum_{n=-\infty}^{\infty} \left[a_n^j J_n(\mathrm{k}_e \mathrm{r}) + b_n^j H_n^{(1)}(\mathrm{k}_e \mathrm{r}) \right] e^{in\theta}, \tag{1}$$

where $k_e = kn_e$. In (1), the Hankel function terms are sourced at the particular cylinder j, while the terms involving Bessel functions of the first kind are due to sources on other cylinders or are associated with an external applied field. On the interior of cylinder j, the general form of the field is

$$V_i(\mathbf{r}+\mathbf{c}^j) = \sum_{n=-\infty}^{\infty} \left[c_n^j J_n(\mathrm{k}_i \mathrm{r}) + q_n^j H_n^{(1)}(\mathrm{k}_i \mathrm{r}) \right] e^{in\theta}, \tag{2}$$

where $k_i = kn_i$. The Bessel function terms associated with coefficients $\{c_n^j\}$ denote the regular part of the field that is source on the cylinder boundary while the Hankel function terms, with coefficients $\{q_n^j\}$, correspond to the field generated by a possible interior source.

2.2. Fictitious Sources: Solution for a single scatterer

We now outline the first of the three key ideas, namely the use of fictitious sources that tailor the field in useful and interesting ways, and which forms the basis of our construction of a defect mode. Beginning with a single scatterer, in which we embed a source

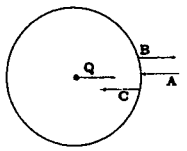

Fig. 2. Field relationships

characterized by coefficients $\mathbf{q}^j = [q_n^j]$, the field inside the cylinder is given by (2), with the exterior field specified by (1). Then, from the continuity conditions that apply at the boundary of the cylinder, we can write the outgoing exterior field and the regular part of the interior field as

$$\mathbf{b}^j = \hat{\mathbf{R}}\mathbf{a}^j + \hat{\mathbf{T}}\mathbf{q}^j, \tag{3}$$

$$\mathbf{c}^j = \hat{\mathbf{T}}'\mathbf{a}^j + \hat{\mathbf{R}}'\mathbf{q}^j. \tag{4}$$

Only the first of these two equations is important to us, with the second being included for completeness. In (3), the source coefficients $\mathbf{b}^j$ are expressed as a reflection ($\hat{\mathbf{R}}$) of the standing wave field $\mathbf{a}^j$ that is incident on the cylinder and a transmission ($\hat{\mathbf{T}}$) through the interface of the interior source $\mathbf{q}^j$. The matrices $\hat{\mathbf{R}}$, $\hat{\mathbf{T}}$, $\hat{\mathbf{R}}'$ and $\hat{\mathbf{T}}'$ are essentially Fresnel coefficients in the cylindrical harmonic basis. Because the local field expansion in cylindrical coordinates is well suited to the circular shape of the scatterers, these matrices are diagonal. If, however, the inclusions were noncircular, then the various matrices would be no longer diagonal, but instead dense.

We are now in a position to construct a defect mode for this simple system. This particular *cylinder may be made to vanish,* as in the case of a defect, *by choosing the fictitious compound source that compensates for the presence of the reflected field.* Making use of Eq. (3), we set $\mathbf{b}^j = \mathbf{0}$ and see that this may be achieved by embedding the fictitious source $\mathbf{q}^j = -\hat{\mathbf{T}}^{-1}\hat{\mathbf{R}}\mathbf{a}^j$ within the cylinder—a source which is dependent on the incident field. This is illustrated in Fig. 3 which shows that exterior field can be can be made identical to the incident field by choosing the appropriate embedded source.

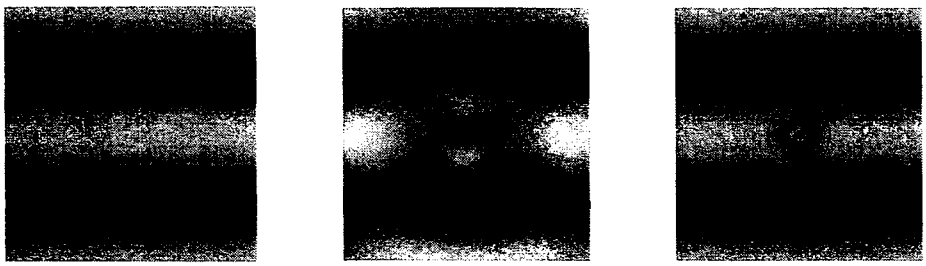

(a) (b) (c)

Fig. 3. Panels (a) and (b) respectively depict the intensity distribution of a plane wave in free space, and a plane wave being diffracted by a dielectric cylinder. In panel (c), we see that the diffracted field outside the cylinder is identical to that in (a) (i.e., in the absence of a scatterer) when an appropriate source is embedded in the cylinder. The field inside the cylinder is non-physical.

While this process is quite straightforward for a single scatterer, the complexity of the interrelationships between scatterers in the full model of a defect mode (with an infinite cladding) makes the direct solution of the problem exceedingly difficult, if not impossible.

2.3. The superposition method

The difficulty of choosing an embedded source in a general situation may be overcome by the *second* of the key ideas, namely the construction of the defect mode from a superposition of solutions of quasiperiodic field problems. We thus embed a source $\mathbf{q}^j = \mathbf{q}\exp\left(i\mathbf{k}_0 \cdot \mathbf{c}^j\right)$ in each cylinder (located at $\mathbf{c}^j$) of the lattice, phased in a quasiperiodic manner. The defect mode is then formed by a superposition of the

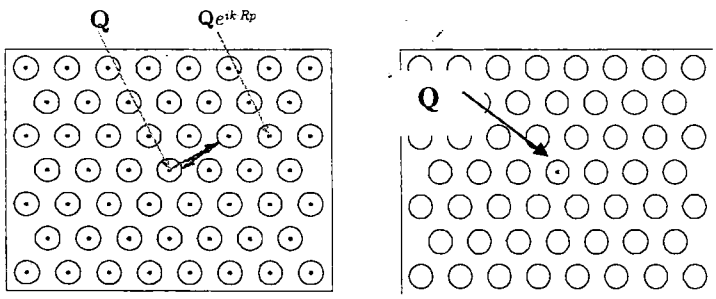

Fig. 4. (a) The quasiperiodic source distribution. (b) After a 2D integration over the Brillouin zone with respect to $\mathbf{k}_0$, only a single source at $\mathbf{r} = \mathbf{r}_0 = \mathbf{0}$ remains.

quasiperiodic field problems by integrating with respect to the Bloch vector $\mathbf{k}_0$ over the first Brillouin zone (BZ) reciprocal lattice.

The superposed solution then satisfies the wave equation and the boundary conditions, and is associated with a fict source distribution which, for cylinder j at $\mathbf{r}=\mathbf{c}^j$ is $\mathbf{q}\int\exp\left(i\mathbf{k}_0\cdot\mathbf{c}^j\right)d\mathbf{k}_0$. This is the key step, with the BZ integ eliminating entirely the fictitious sources in all but the primary cylinder ($j=0$). The sole remaining sour $\mathbf{r}=\mathbf{r}_0=\mathbf{0}$ is thus available to modify the response field and, in doing so, to formulate the defect mode.

In the case of 2D lattices, the integration over the Brillouin zone requires the calculation of a computationally expensive double integral. This efficiency problem can be overcome, however, by reformulating the problem so that only a one-dimensional integration is required. The reformulation is the *third* key idea, modeling the structure as a diffraction grating with an embedded quasiperiodically phased line of sources (Fig. 5) sandwiched between two semi-infinite photonic crystals, the properties of which are modeled by the Fresnel reflection matrix $\mathbf{R}_\infty$ [7,8]. Our use of $\mathbf{R}_\infty$ is crucial in that it encapsulates the second dimension of the BZ, eliminating one integration and simplifying the solution of the problem to require only a one-dimensional BZ integration.

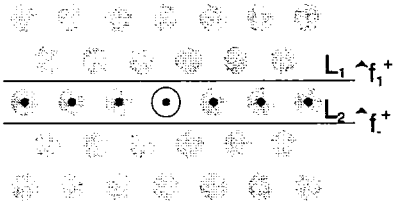

Fig. 5. Geometry of the model showing the grating and its fictitious sources, the defect (i.e., the cylinder to be removed) and the plane wave fields.

The following section digresses to reformulate the problem in terms of the grating model, after which we return to t construction of the defect mode.

2.4. Reformulation in terms of a diffraction grating model

We now consider a cylinder grating with embedded quasiperiodically phased sources and note, from Bloch's theore that $V(\mathbf{r}+d\hat{\mathbf{x}})=V(\mathbf{r})\exp(i\alpha_0 d)$ where α_0 is the lateral component of the Bloch vector $\mathbf{k}_0$. From this quasiperiodicit it follows that the coefficients in the multipole expansions (1) and (2) for cylinder j are given by

$$\mathbf{a}^j=\mathbf{a}e^{i\alpha_0 jd},\qquad \mathbf{b}^j=\mathbf{b}e^{i\alpha_0 jd},\qquad \mathbf{c}^j=\mathbf{c}e^{i\alpha_0 jd},\qquad \mathbf{d}^j=\mathbf{d}e^{i\alpha_0 jd} \tag{5}$$

From (1), we see that the exterior field expansion is determined by the singular and non-singular parts of the field whic are related by a field relation known as the Rayleigh identity. In physical terms, this states that the non-singular part c the field is due to sources radiating from all other cylinders (of the grating) and to sources that are exterior to the grat ing. The derivation of the exact form of the Rayleigh identity that is appropriate in this case requires the use of a Gree function satisfying the inhomogeneous Helmholtz equation

$$(\nabla^2+k^2)G(\mathbf{r})=\sum_{j=-\infty}^{\infty}\delta(\mathbf{r}-jd\hat{\mathbf{x}})e^{i\alpha_0 d}, \tag{6}$$

the solution of which is

$$\begin{aligned}G(r)&=\frac{-i}{4}\sum_{j=-\infty}^{\infty}H_0^{(1)}(k_e\,|\,\mathbf{r}-jd\hat{\mathbf{x}}\,|)e^{i\alpha_0 jd}\\&=\frac{-i}{4}H_0^{(1)}(k_e r)-\frac{-i}{4}\sum_{j=-\infty}^{\infty}S_l J_l(k_e r)e^{il\theta}.\end{aligned} \tag{7}$$

In (7), the S_l are *lattice sums*

$$S_l=\sum_{\substack{j=-\infty,\\ j\neq 0}}^{\infty}H_l^{(1)}(k_e\,|\,j\,|\,d)e^{i\arg(j)}e^{i\alpha_0 jd}, \tag{8}$$

that characterize the contributions to each multipole order due to the (linear) phased array of multipole sources that represents the grating. Later, we will also make use of an alternative form of the Green's function,

$$G(\mathbf{r}) = \sum_{q=-\infty}^{\infty} \chi_q^{-1} e^{i(\alpha_q x + \chi_q |y|)} \text{ where } \alpha_q = \alpha_0 + \frac{2\pi q}{d}, \text{ and } \chi_q = \sqrt{k_e^2 - \alpha_q^2}, \tag{9}$$

this time involving the plane wave basis in which the direction sines and cosines of the plane waves are given by $\sin\theta_q = \alpha_q / k_e$, $\cos\theta_q = \chi_q / k_e$ respectively.

We next formulate the field in the vicinity of the primary cylinder using an application of Green's Theorem

$$V(r) = I(C) + I(D) \quad \text{where} \quad I(P) = \oint_P G(\mathbf{r}-\mathbf{r}') \frac{\partial V}{dn'}(\mathbf{r}') - \frac{\partial G}{dn'}(\mathbf{r}-\mathbf{r}') V(\mathbf{r}')\, ds', \tag{10}$$

where the two line integrals run over the exterior boundary of the cylinder C and the boundary of the unit cell D. We evaluate these two line integrals, respectively using the multipole representation (7) of the Green's function for $I(C)$ and the plane wave form (9) of the Green's function for $I(D)$, and derive

$$\begin{aligned} I(C) &= \sum_l b_l H_l^{(1)}(\mathrm{k_e r}) e^{il\theta} + \sum_l J_l(\mathrm{k_e r}) e^{il\theta} \sum_m S_{l-m} b_m, \\ I(D) &= \sum_{p=-\infty}^{\infty} \chi_p^{-1/2} \left(f_{1p}^- e^{i\chi_p y} + f_{2p}^+ e^{+i\chi_p y} \right) e^{i\alpha_p x}. \end{aligned} \tag{11}$$

The integral around contour D represents the source of incoming plane waves leading to the expression in (11). Correspondingly for $I(C)$, the multipole form of the Green's function (7), which comprises two terms, gives rise to an outgoing field (i.e., the Hankel function terms) from cylinder C and standing wave terms (i.e., the Bessel function terms) that are generated by all other cylinders of the grating. Finally, converting the plane wave terms in $I(D)$ into the cylindrical harmonic basis with the aid of the Bessel generating function, we deduce the field identity connecting the coefficients in the multipole representation of the field

$$V(\mathbf{r}) = \sum_l \left(a_l J_l(\mathrm{k_e r}) + b_l H_l^{(1)}(\mathrm{k_e r}) \right) e^{il\theta}. \tag{12}$$

Thus, we deduce

$$a_l = \sum_{m=-\infty}^{\infty} S_{lm} b_m + \sum_{p=-\infty}^{\infty} J_{0lp}^- f_{1p}^- + J_{0lp}^+ f_{2p}^+, \tag{13}$$

where $S_{lm} = S_{l-m}$, $J_{0lp}^- = \chi_p^{-1/2} e^{il\theta_p}$ and $J_{0lp}^+ = \chi_p^{-1/2} (-1)^l e^{-il\theta_p}$. In matrix notation, this reduces to

$$\mathbf{a} = \mathbf{S}\mathbf{b} + \mathbf{J}_0^- \mathbf{f}_1^- + \mathbf{J}_0^+ \mathbf{f}_2^+, \tag{14}$$

and indicates that the regular (non-singular) part ($\mathbf{a}$) of the multipole field in the vicinity of the primary cylinder is due to outgoing radiation from all the cylinders of the grating ($\mathbf{Sb}$) and to the incoming plane wave fields from above ($\mathbf{J}_0^- \mathbf{f}_1^-$) and below ($\mathbf{J}_0^+ \mathbf{f}_2^+$). In (14), the matrices $\mathbf{J}_0^{\pm}$ effectively perform a change of basis converting upward and downward propagating plane waves into the cylindrical harmonic basis. Combining this with the boundary conditions (3), we are led to express the source coefficients ($\mathbf{b}$) in terms of the embedded fictitious sources and the incident plane wave terms

$$\mathbf{b} = \mathbf{G}\left(\hat{\mathbf{R}} \mathbf{J}_0^- \mathbf{f}_1^- + \hat{\mathbf{R}} \mathbf{J}_0^+ \mathbf{f}_2^+ + \hat{\mathbf{T}} \mathbf{q} \right), \text{ where } \mathbf{G} = \left(\mathbf{I} - \hat{\mathbf{R}} \mathbf{S} \right)^{-1} \tag{15}$$

It is important to recognize that since the field sources lie within the grating, the incoming plane wave fields in (15) are due to reflections from the semi-infinite photonic crystal arrays (above and below the grating) of outgoing plane wave fields sourced by the grating. These outgoing plane wave fields comprise two parts: an incident specular field that passes straight through the grating and a scattered field term that is sourced by the grating. The precise form of the latter follows from evaluating the integral $I(C)$, this time using the plane wave form of Green's function (9), since $I(C)$ generates the field that is outgoing from the grating. We thus derive

$$f_{1p}^- = f_{2p}^- + K_{0pl}^+ B_l, \; f_{2p}^- = f_{1p}^- + K_{0pl}^- B_l \quad \text{where} \quad K_{0pl}^+ = \frac{2}{d} \chi_p^{-1/2} e^{-il\theta_p}, \; K_{0pl}^- = \frac{2}{d} \chi_p^{-1/2} (-1)^l e^{il\theta_p}, \tag{16}$$

or, in matrix form,

$$\mathbf{f}_1^+ = \mathbf{f}_2^+ + \mathbf{K}_0^+\mathbf{b},\ \mathbf{f}_2^- = \mathbf{f}_1^- + \mathbf{K}_0^-\mathbf{b}.$$

The matrices $\mathbf{K}_0^\pm$ again perform a change of basis (essentially the reverse of that associated with $\mathbf{J}_0^\pm$), this time cylindrical harmonics to plane waves. Combining the results in (15) and (17), we are led to the following expres for the outgoing plane wave fields above and below the grating

$$\mathbf{f}_1^+ = \mathbf{R}_0^+\mathbf{f}_1^- + \mathbf{T}_0^+\mathbf{f}_2^+ + \mathbf{Q}_0^+\mathbf{q},$$
$$\mathbf{f}_2^- = \mathbf{T}_0^-\mathbf{f}_1^- + \mathbf{R}_0^-\mathbf{f}_2^+ + \mathbf{Q}_0^-\mathbf{q},$$

where $\mathbf{R}_0^+ = \mathbf{K}_0^+\mathbf{G}\hat{\mathbf{R}}\mathbf{J}_0^-$, $\mathbf{R}_0^- = \mathbf{K}_0^-\mathbf{G}\hat{\mathbf{R}}\mathbf{J}_0^+$, $\mathbf{T}_0^+ = \mathbf{I} + \mathbf{K}_0^+\mathbf{G}\hat{\mathbf{R}}\mathbf{J}_0^+$, $\mathbf{T}_0^- = \mathbf{I} + \mathbf{K}_0^-\mathbf{G}\hat{\mathbf{R}}\mathbf{J}_0^-$, $\mathbf{Q}_0^+ = \mathbf{K}_0^+\mathbf{G}\hat{\mathbf{T}}$, $\mathbf{Q}_0^+ = \mathbf{K}_0^-\mathbf{G}\hat{\mathbf{T}}$. We see from (18), that in the absence of an embedded source (i.e., with $\mathbf{q} = \mathbf{0}$), the terms $\mathbf{R}_0^\pm$ and $\mathbf{T}_0^\pm$ are the plane wave reflection and transmission scattering matrices of the grating for incidence from above and below. The terms $\mathbf{Q}_0^\pm\mathbf{q}$ refer to the contributions to the upward and downward going plane wave fields that are generated by the embedded source.

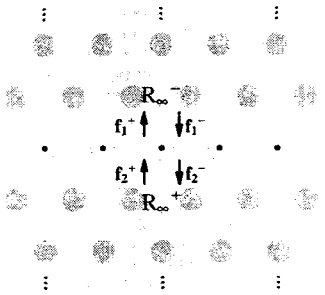

Fig. 6. Schematic of the structure mo eled, showing a sourced grating em- bedded between semi-infinite photoni crystals, and the plane wave fields, respectively sourced at the grating an reflected by the PC "mirrors" above and below.

2.5. Modeling of the semi-infinite mirrors

We now consider the properties of the semi-infinite stacks above and below the grating and note that for complete modal confinement, the bulk crystals that constitute these stacks need to be operated in a band gap—otherwise the existence of propagating states in the infinite cladding would preclude a defect state. The aim here is to characterize the reflection of the semi-infinite crystal in terms of plane wave scattering matrices $\mathbf{R}_\infty^\pm$, where $\mathbf{f}_1^- = \mathbf{R}_\infty^-\mathbf{f}_1^+$ and $\mathbf{f}_2^+ = \mathbf{R}_\infty^+\mathbf{f}_2^-$.

This we undertake by computing the Bloch modes of the bulk crystal using a transfer matrix method [7,8] where v solve the eigenvalue problem

$$\mathcal{T}\begin{pmatrix}\mathbf{f}^-\\ \mathbf{f}^+\end{pmatrix} = \mu\begin{pmatrix}\mathbf{f}^-\\ \mathbf{f}^+\end{pmatrix},\ \text{where}\ \mathcal{T} = \begin{pmatrix}\mathbf{T}-\mathbf{R}'\mathbf{T}'^{-1}\mathbf{R} & \mathbf{R}'\mathbf{T}'^{-1}\\ -\mathbf{T}'^{-1}\mathbf{R} & \mathbf{T}'^{-1}\end{pmatrix} \tag{1'}$$

to determine the vectors $\mathbf{f}_\pm$ in the plane wave expansion

$$V(\mathbf{r}) = \sum_{p=-\infty}^{\infty} \chi_p^{-1/2}\left[f_p^- e^{-i\chi_p y} + f_p^+ e^{i\chi_p y}\right]e^{i\alpha_p x} \tag{2(}$$

of the Bloch modes along the interlayer boundaries The form of the transfer matrix must be consistent with the struc ture of the lattice and so, in (19), the scattering matrices $\mathbf{R}$, $\mathbf{T}$, $\mathbf{R}'$ and $\mathbf{T}'$, are derived from the grating scatterin matrices $\mathbf{R}_0^\pm$ and $\mathbf{T}_0^\pm$ by applying geometric transformations that pad the layers to the correct thickness and shear th unit cell to be the correct shape, consistent with the lattice vectors, by altering the field phase origins at the upper an lower interfaces according to

$$\begin{pmatrix}\mathbf{T} & \mathbf{R}'\\ \mathbf{R} & \mathbf{T}'\end{pmatrix} = \mathcal{Q}^{1/2}\mathcal{P}^{1/2}\begin{pmatrix}\mathbf{T}_0^- & \mathbf{R}_0^-\\ \mathbf{R}_0^+ & \mathbf{T}_0^+\end{pmatrix}\mathcal{P}^{1/2}\mathcal{Q}^{1/2},$$
$$\text{where}\ \mathcal{P} = \begin{pmatrix}\mathbf{P} & 0\\ 0 & \mathbf{P}\end{pmatrix},\ \mathcal{Q} = \begin{pmatrix}\mathbf{Q}^{-1} & 0\\ 0 & \mathbf{Q}\end{pmatrix} \tag{21}$$

and $\mathbf{Q} = \operatorname{diag}\exp(i\alpha_p s_x)$ and $\mathbf{P} = \operatorname{diag}\exp(i\chi_p s_y)$, where s_x and s_y are the components of the lattice vecto $\mathbf{e}_2 = (s_x, s_y)$. Note that for a square lattice, $\mathbf{e}_1 = d(1,0)$ and $\mathbf{e}_2 = d(1,0)$, while for a hexagonal lattice, $\mathbf{e}_1 = d(1,0)$ and $\mathbf{e}_2 = d(1,\sqrt{3})/2$.

Truncating the matrices appropriately and solving (19), we derive a set of modes $\left[\mathbf{f}_j^{-T}, \mathbf{f}_j^{+T}\right]$ and Bloch factors $\mu = \exp(-i\mathbf{k}_0 \bullet \mathbf{e}_2)$ which may be partitioned into downward and upward propagating sets, and which are paired by reciprocity and energy conservation arguments [5,8]. In the case of the downward propagating modes, we combine the vectors $\mathbf{f}^{\pm}$ columnwise to form matrices $\mathbf{F}^{\pm}$. Correspondingly, we can assemble the upward propagating modes columnwise into matrices $\mathbf{F}'^{\pm}$.

From here, it is a straightforward matter to calculate the reflection matrices $\mathbf{R}_{\infty}^{\pm}$ for the semi-infinite PCs, for incidence from above and below. In the case of a field $\mathbf{f}_2^-$, incident from above onto a semi-infinite PC, giving rise to a reflected field $\mathbf{f}_2^+$, we may express the field matching condition at the interface with the PC as

$$\begin{pmatrix} \mathbf{f}_2^- \\ \mathbf{f}_2^+ \end{pmatrix} = \begin{pmatrix} \mathbf{F}^- \\ \mathbf{F}^+ \end{pmatrix} \mathbf{c}^- \tag{22}$$

with the right hand side of (22) representing a linear combination of downward propagating Bloch modes with amplitudes $\mathbf{c}^- = \left[\mathbf{c}_n^-\right]$. The Bloch mode expansion in (22) contains no upward propagating modes since the slab is semi-infinite and there are no sources of upward propagating modes. Then, eliminating $\mathbf{c}^-$, we deduce that

$$\mathbf{f}_2^+ = \mathbf{R}_{\infty}^+ \mathbf{f}_2^- \quad \text{where} \quad \mathbf{R}_{\infty}^+ = \mathbf{F}^+ \left(\mathbf{F}^-\right)^{-1}. \tag{23}$$

The reflection matrix $\mathbf{R}_{\infty}^-$ may be found in a similar manner and using symmetry arguments it may be shown that for square and hexagonal arrays

$$\mathbf{R}_{\infty}^+ = \mathbf{R}_{\infty}^- = \mathbf{R}_{\infty}. \tag{24}$$

The construction of the matrix $\mathbf{R}_{\infty}$ outlined above is straightforward in that it involves the solution of systems of linear equations of full rank. Typically, in these calculations, we truncate the plane wave series to include terms with indices $p \in [-5,5]$ or less, thus generating matrices whose dimension is 11×11 or smaller. Bloch mode methods are also widely used in device design [9,10,11] which requires the device being modeled as being encapsulated in a supercell whose width is sufficiently large to ensure that adjacent supercells are effectively isolated from one another. In such cases the matrices that arise are much larger—a consequence of the size of the supercell and also the effective spatial resolution that is required of the plane wave series. In some cases, however, it is desirable to work with a truncated basis of modes in order to capture cleanly the essential physics of the problem which may be associated with only relatively few modes. The field matching equations (such as (22)) are then no longer exact, in the sense that the dimension of the modal basis is less than the dimension of the plane wave basis. In such circumstances, these need to be solved in a least squares sense. This can be achieved in a computationally attractive and analytically elegant manner by means of orthogonality relations that emerge from physical constraints such as reciprocity and energy conservation. The derivation of these is somewhat lengthy and so we present only the results, referring the interested reader to [5,8] for the full treatment. For the modes of the bulk crystal that are dealt with in this paper, the two key results are

$$\mathcal{F}^T S_{\mathrm{pw}} \mathcal{F} = S_{\mathrm{bm}}, \quad \mathcal{F}^H \mathcal{J}_{\mathrm{pw}} \mathcal{F} = \mathcal{J}_{\mathrm{bm}}. \tag{25}$$

These follow respectively from reciprocity and energy conservation and mirror the corresponding properties that are satisfied by the transfer matrices

$$\mathcal{T}^T S_{\mathrm{pw}} \mathcal{T} = S_{\mathrm{bm}}, \quad \mathcal{T}^H \mathcal{J}_{\mathrm{pw}} \mathcal{T} = \mathcal{J}_{\mathrm{bm}}. \tag{26}$$

In (25) and (26), we have

$$\mathcal{F} = \begin{pmatrix} \mathbf{F}^- & \mathbf{F}^+ \\ \mathbf{F}^+ & \mathbf{F}^- \end{pmatrix}, \quad S_q = \begin{pmatrix} \mathbf{0} & \mathbf{I} \\ -\mathbf{I} & \mathbf{0} \end{pmatrix}, \quad \mathcal{J}_q = \begin{pmatrix} \mathbf{I}_q & -i\mathbf{I}_{\bar{q}} \\ i\mathbf{I}_{\bar{q}} & -\mathbf{I}_q \end{pmatrix} \tag{27}$$

It is important to note that since the reciprocity theorem is geometrical in its origin, it is universally applicable. However, the results which derive from energy conservation are applicable only to lossless systems.

2.6. Formulation of the defect mode

The reflection conditions derived at the end of the previous section

$$\mathbf{f}_1^- = \mathbf{R}_\infty^- \mathbf{f}_1^+ \quad \text{and} \quad \mathbf{f}_2^+ = \mathbf{R}_\infty^+ \mathbf{f}_2^-$$

together with the outgoing plane wave form (18) and the representation for the multipole coefficients $\mathbf{b}$ express terms of the incoming plane wave and fictitious source quantities (15) allows us to derive the homogenous form

$$\mathbf{b} = \mathbf{Z}\mathbf{q}$$

which expresses the outgoing field around the primary cylinder in terms of the fictitious source that it contains. $\mathbf{Z}$ is a function of both wavenumber k and Bloch vector component α_0, i.e., $\mathbf{Z} = \mathbf{Z}(k, \alpha_0)$ where

$$\mathbf{Z} = \frac{1}{2}\mathbf{G}\{\hat{\mathbf{R}}\left(\mathbf{J}_0^- + \mathbf{J}_0^+\right)\left[\mathbf{I} - \mathbf{R}_\infty\left(\mathbf{R}_0 + \mathbf{T}_0\right)\right]^{-1}\mathbf{R}_\infty\left(\mathbf{Q}_0^+ + \mathbf{Q}_0^-\right) +$$
$$+\hat{\mathbf{R}}\left(\mathbf{J}_0^- - \mathbf{J}_0^+\right)\left[\mathbf{I} - \mathbf{R}_\infty\left(\mathbf{R}_0 - \mathbf{T}_0\right)\right]^{-1}\mathbf{R}_\infty\left(\mathbf{Q}_0^+ - \mathbf{Q}_0^-\right) + \hat{\mathbf{T}}\}.$$

We can make immediate use of (29) to construct the modes of a simple waveguide. To understand this, imagine tha set $\mathbf{b} = \mathbf{0}$ as before, thus zeroing the outgoing field scattered by the primary cylinder. Because of the Bloch conditi the outgoing field in the vicinity of each cylinder j also vanishes since $\mathbf{b}_j = \mathbf{b}\exp(ij\alpha_0 d) = \mathbf{0}$. Thus, by setting $\mathbf{b}$ = we eliminate the entire row of cylinders, thereby forming a waveguide. The mode is then given by the non-trivial s tion of the homogeneous system of equations

$$\mathbf{Z}\mathbf{q} = \mathbf{0} \qquad (3$$

which we locate for a given frequency k by scanning the Brillouin zone by varying the Bloch vector component over the interval $[-\pi/d, \pi/d]$ to locate a root of the equation

$$\det \mathbf{Z}(k, \alpha_0) = 0. \qquad (3$$

The dispersion curve then follows by repeating this procedure over a designated frequency range. Furthermore, the tual mode may be reconstructed from the corresponding null vectors of $\mathbf{Z}$.

A simple extension of this technique enables us to modify the central row of cylinders, represented by the gratii Physically, this may involve altering the cylinder radius, the refractive index or even the shape of the cylinder. In cases, we model the altered characteristics by a reflection matrix $\hat{\mathbf{R}}_1$, such that for an incident multipole field $\mathbf{a}$, t outgoing field from the altered cylinder is $\mathbf{b} = \hat{\mathbf{R}}_1\mathbf{a}$. Since this modification is to be generated by a fictitious source within the original cylinder, we must have $\mathbf{b} = \hat{\mathbf{R}}\mathbf{a} + \hat{\mathbf{T}}\mathbf{q}$ where $\hat{\mathbf{R}}$ and $\hat{\mathbf{T}}$ are the multipole reflection and transmissi matrices of the original cylinder as before. Finally, we invoke the relationship (29) derived above and form the dispe sion relation for this modified waveguide by solving the homogeneous system of equations

$$\left[\left(\mathbf{I} - \hat{\mathbf{R}}_1\hat{\mathbf{R}}^{-1}\right)\mathbf{Z} + \hat{\mathbf{R}}_1\hat{\mathbf{R}}^{-1}\hat{\mathbf{T}}\right]\mathbf{q} = \mathbf{0} \qquad (3$$

in the same way as outlined immediately above (32).

The remaining step is to form the two-dimensional defect mode from a superposition of solutions of the problem associ ated with a linear array of sources that are quasi-periodically phased. We begin with the relation $\mathbf{b}(k, \alpha_0) = \mathbf{Z}(k, \alpha_0)\mathbf{q}$ and observe that for cylinder j which is associated with the source $\mathbf{q}^j(\alpha_0) = \mathbf{q}\exp(ij\alpha_0 d)$, the corresponding multipol source coefficients are $\mathbf{b}^j(k, \alpha_0) = \mathbf{b}(k, \alpha_0)\exp(ij\alpha_0 d)$. When we superpose all solutions by integrating ove $\alpha_0 \in [-\pi/d, \pi/d]$, only a single source associated with the primary cylinder remains, since $< \mathbf{q}^j(\alpha_0) >= \mathbf{q}\,\delta_{j0}$, where the averaging operator is defined by

$$< f >= \frac{1}{d}\int_{-\pi/d}^{\pi/d} f(\alpha_0)\, d\alpha_0. \qquad (34)$$

To construct the 2D defect mode, we set $< \mathbf{b}^0(k, \alpha_0) >= 0$ and require a solution of

$$\langle \mathbf{Z}(k) \rangle \mathbf{q} = \mathbf{0} \quad \text{where} \quad \langle \mathbf{Z}(k) \rangle = \int_{-\pi/d}^{\pi/d} \mathbf{Z}(k, \alpha_0)\, d\alpha_0 \qquad (35)$$

by searching for roots k of the equation $\det < \mathbf{Z}(k) > = 0$.

The theory, as outlined above, pertains to a two-dimensional problem for either of the two fundamental polarizations. Its extension to three-dimensional fields, which are vector in nature, and which accommodate out-of-plane propagation with a spatial dependence of $\exp(i\beta z)$, is quite straightforward and is outlined in [4]. The overall structure of the formulation is identical, with only the nature of the search routine for the roots of the dispersion equation being altered to suit the problem being tackled. In the case of a search for modes of a MOF, the defect acts as the fiber core and β corresponds to the propagation constant of the mode, and we look for roots of $\det < \mathbf{Z}(k, \beta) > = 0$ which prescribe the dispersion equation $n_{\text{eff}} = n_{\text{eff}}(k)$ where $n_{\text{eff}} = \beta / k$.

2.7. Verification

We have validated the method by testing it against alternative techniques (including the commercial software RSoft BandSolve) for computing waveguide modes and field modes in photonic crystal fibers. In all cases, the method generates results of high accuracy in a very efficient manner. Exemplifying this is the computation of the fundamental mode of a MOF using this (FSS) method and the multipole utilities developed within our group [12,13,14]. The agreement between the two calculations shown in Fig. 7 is excellent, as is the agreement between the calculations of the effective refractive index. The FSS method estimates $n_{\text{eff}} = 1.4493364513$ while the CUDOS MOF utilities [14] estimate that for a finite structure with seven rings of holes $n_{\text{eff}} = 1.4493364520 + i1\times10^{-12}$, where the small imaginary part corresponds to the leakage associated with the finite size.

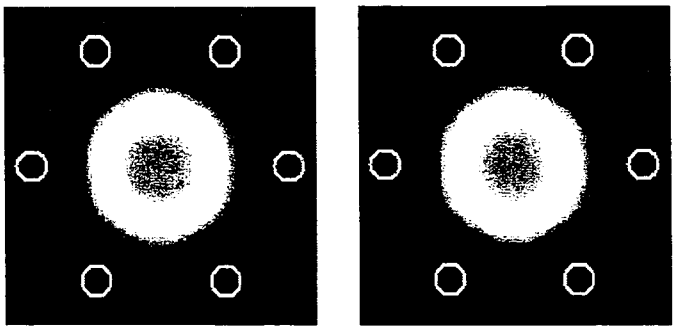

Fig. 7. Axial component of the Poynting vector for the fundamental mode of a hexagonal MOF with a single cylinder defect at wavelength $\lambda / d = 0.133$. The structure has air holes of normalized radius $a / d = 0.2$ in glass of refractive index $n = 1.45$. The left panel shows the mode reconstructed using the FSS method, while the right panel uses the CUDOS MOF (multipole) Utilities in which the structure is modelled as having 7 rings of holes. .

While the above example, for a well confined mode, demonstrates that the FSS method can replicate results from other methods whose accuracy, and limits of accuracy, are well known, it does not bring out the real potential of the method, designed to handle the more challenging problem of modeling extended modes such as occur near cutoff or near the edge of a band gap. Accordingly, in our next example (Fig. 8), we consider a highly extended mode formed using a square lattice (with lattice constant d) having cylinders of radius $a / d = 0.2$ and refractive index of $n = 3.0$ in a background medium of index $n = 1$, with the central cylinder replaced by one of radius $a / d = 0.17$. Using a 40 point Gaussian integration rule we were able to find, within three minutes, a defect mode at a normalized frequency of $d / \lambda = 0.32103515465$ which subsequent convergence studies showed was accurate to 11 significant figures. While this mode can also be found using the commercial software RSoft BandSolve (which uses a supercell method based on plane wave expansions) in a similar time, the same accuracy cannot be achieved.

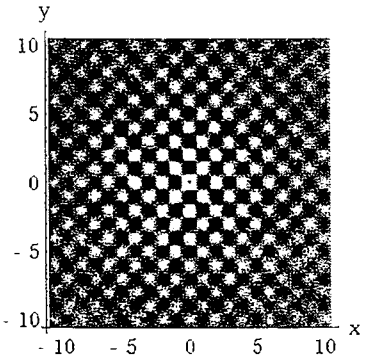

Fig. 8. Electric field intensity in an E polarized defect mode in a square lattice with $a / d = 0.2$, the central cylinder of which has been replaced by one of normalized radius 0.17

3. LONG WAVELENGTH PROPERTIES OF FUNDAMENTAL MODE IN INDEX-GUIDED MOF

While the modes and their cut-offs in conventional step-index fibers are well understood, the situation for index guided photonic crystal fibers (PCF) is less clear, particularly as the problem has no closed-form solutions. In all of the previ-

ous theoretical work, the problem has been solved for problems which are subtly different using either supercell ods or modeling a finite structure [15].

Previously, our group investigated the long wavelength behavior of the fundamental mode by considering a MOI finite cladding, and then extrapolating the results to structures with infinite cladding [2]. In these, the medium oi the microstructured cladding was taken to be solid glass and it was found that in MOFs with finite cladding, the r area is limited to the core at short wavelengths, and covers the entire cladding cross section at long wavelengths. tween these extremes, the modal area grows rapidly with wavelength, a process that is associated with strongly inc ing confinement losses. In contrast with the behavior of the second mode [3], an extrapolation procedure showec the width of this transition region remained finite in the limit that the cladding becomes infinite, leading to a some controversial interpretation that a cut-off did exist for the fundamental MOF mode [2]. The need to clarify the exis or otherwise of the "cut-off", in fact, motivated the development of the FSS method [4,16].

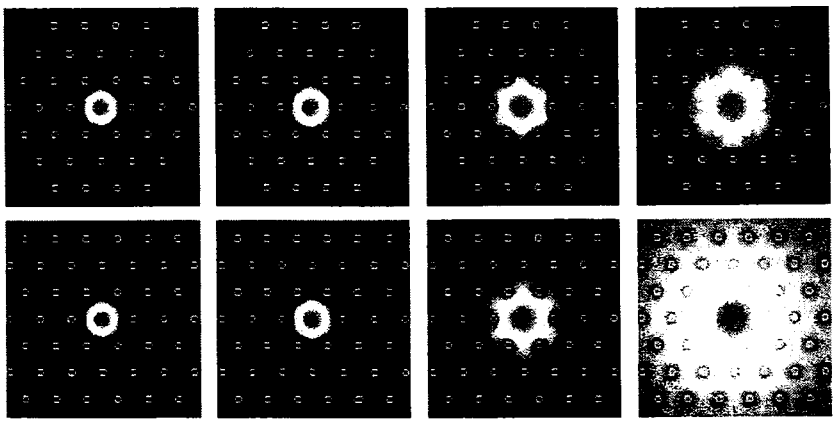

$\lambda/d = 0.133$ $\lambda/d = 0.5$ $\lambda/d = 1.1$ $\lambda/d = 1.6$

Fig. 9. Axial component of the Poynting vector for a finite PCF with a 3 ring cladding (top row) and PCF with an infinite cladding (bottom row) for the specified wavelengths.

The first of the results obtained using the FSS method are presented in Figs 9 which shows contour maps of the ax component of the Poynting vector for the fundamental mode of a hexagonal MOF with $a/d = 0.12$ and backgrou refractive index $n = 1.45$. The lower row shows results for an infinite cladding while, in the upper row, results fo finite structure with a three ring cladding are presented. The various columns correspond to different wavelengths, i creasing from left to right. The wavelengths have been chosen to accord with the results for a finite MOF [2] for whi at λ/d=0.133 the fundamental mode exists, while for λ/d=1.1 and λ/d=1.6 the mode is cut off. The intermedia wavelength shown, λ/d=0.5, corresponds to the transition region. It is clear from Figs 9 that the mode does not cut c at the longest wavelengths, in contrast to the conclusions reached earlier [2]. Note further that only at the longest wav lengths do the energy density in the infinite and finite cladding MOFs differ significantly, and that the field in the fib with finite cladding is actually better confined than that in the structure with the infinite cladding [17].

In order to study the cutoff of the fundamental mode in more detail we consider Figs 10, in which the left-hand pan shows the difference of the effective mode index n_{eff} and the effective index of the fundamental space filling mod n_{fsm}, the latter playing the same role as the cladding refractive index in conventional guided-wave structures [1]. Ind cated are results for structures with a infinite cladding (solid curve), as well as structures with a finite cladding (long and short-dashed curves). When $n_{\text{eff}} > n_{\text{fsm}}$ the field in the cladding region is evanescent, whereas otherwise it is propa gating. At short wavelengths, the effective indices of the fundamental modes in all structures are roughly the same, an well above n_{fsm}. This is because the field is confined strongly to the core, decaying substantially when it reaches th outer edge of the cladding.

Significant differences between the MOFs with finite and infinite cladding become apparent at longer wavelengths. In the MOF with the infinite cladding, as the wavelength increases, the effective index of the mode approaches n_{fsm} from above, but never crosses it. This indicates that, in the infinite structure, the fundamental mode is always evanescent in the cladding. It is thus always guided and does not cut off, consistent with the conclusion from Figs 9. The behavior of the structures with finite cladding is different: as the wavelength increases, they deviate from each other, and eventually drop below n_{fsm}, indicating that the field is not evanescent in the cladding region. Indeed, the losses of these modes (not shown here) increase rapidly to the point where confinement is effectively lost [2].

The long wavelength behavior for MOFs should be compared with that of a w-fiber, a conventional fiber in which the core is surrounded by a finite ring of low refractive index, which, in turn, is surrounded by a region with the same refractive index as the core (right-hand side of Figs 10). It thus has a finite cladding and is the equivalent of the fiber we have considered thus far, but consists of piecewise uniform material. The right-hand side of Figs 10 gives the same information as the figure on the left, i.e., it shows the effective index of the fundamental mode for structures with infinite (solid) and finite (long- and short-dashed lines) cladding. The only difference is that n_{fsm} is now replaced by the constant cladding refractive index. From the similarity of the two figures, we conclude that the cut-off behavior of the fundamental modes of MOF structures and of w-fibers, are qualitatively the same. This conclusion is strongly supported by considering the field plots in the w-fiber, essentially the equivalents of Figs 9. However, we do not show these results [16] here.

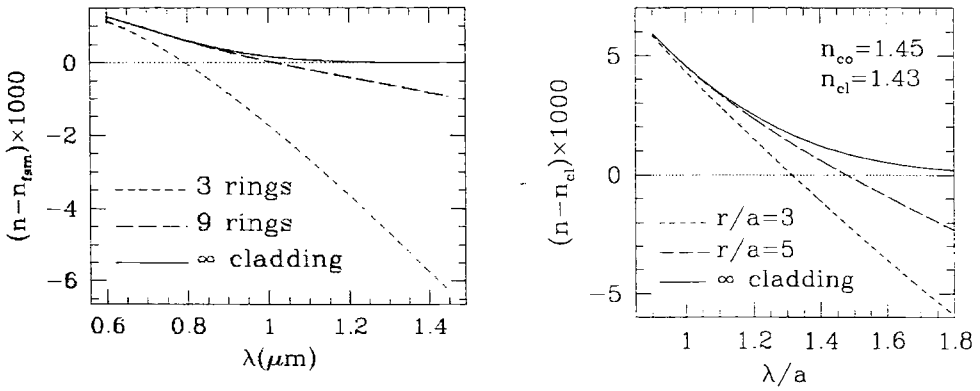

Fig 10. Left: difference of the effective refractive indices of the fundamental mode in a PCF with infinite cladding (solid curve), and a finite cladding of 9 rings (long-dashed) and 3 rings (short-dashed), and the effective index of the fundamental space filling mode n_{fsm}. The PCF parameters are the same as for those for Figs 9. The dotted line, indicating the zero level, is included for convenience. Right: corresponding results for a w-fiber, the conventional equivalent. The core of this fiber has a radius a and a refractive index $n=1.45$. The cladding has a radius r and a refractive index $n=1.43$. The region outside the cladding has a refractive index $n=1.45$.

Even though we have found that the fundamental mode in a index-guided MOF does not have a cutoff, the existence of the transition region, found from the properties of MOFs with finite cladding [3], is genuine. One may ask the significance of this region in light of the results obtained for MOFs with infinite cladding. Preliminary results show that this region is to be interpreted as the wavelength interval over which the fundamental mode's spatial extent increases significantly.

We are therefore led to conclude that at long wavelengths, index-guided MOFs behave similarly to conventional fibers [18]. Of course this is not true at short wavelengths, where MOFs can exhibit endlessly single-mode behavior [1,2]. The analogy with conventional fibers can be straightforwardly analyzed quantitatively; even at $\lambda/d=1.6$, the longest wavelength considered here, $n_b-n_{\text{fsm}}\approx 0.023$, where n_b is the refractive in the core. We can therefore understand the dominant field component of the mode using the scalar approximation [19]. We find that at this wavelength the transverse wavevector $k_\perp$ has a small value such that $k_\perp d\approx 7\times 10^{-3}$. In analogy with conventional fibers, therefore, we expect the

field of the fundamental mode in the cladding to vary, on average, as $K_0(k_\perp r)$, where K_0 is a modified Bessel fu We have confirmed this numerically. We may use this approximation to estimate the effective mode size. Doing can estimate the approximate radius $r_{1/2}$ where the average field intensity decays to half the value at the core edge by $\rho = d/\sqrt{3}$ [18]. At $\lambda/d = 1.6$, we find that $r_{1/2} \approx 200d$, so the mode field extends over hundreds of periods; knowledge, no conventional computational method exists that can be used to calculate such large modes.

4. DISCUSSION AND CONCLUSIONS

We have developed the FSS method in order to calculate the properties of infinite structures that are periodic, apar a localized defect. In a sense this is a generalization of our previous work in which we used the matrix $\mathbf{R}_\infty$ [7,8] termine the properties of line defects in otherwise genuinely infinite periodic structures. In these calculations $\mathbf{R}_\infty$ acterizes the media on either side of the waveguide. In a sense, the calculation here, which is for point defects, s how to "surround" the defect by a periodic structure on all four sides, rather than at just two. One may query the that the method in fact calculates the properties of genuinely infinite structures. The answer to this question hing the Brillouin zone integration described in Sec. 2.6. While the use of an elementary integration rule like the rect rule is, in effect, equivalent to periodic boundary conditions in the associated directions, this conclusion cann drawn for more complicated integration rules such as Gaussian integration. In our calculations we have used a nu of different integration rules and have obtained essentially the same results each time. We therefore conclude tha calculations indeed do give results for a genuinely infinite cladding.

Further, our method has allowed the first rigorous study of the long wavelength behavior of a MOF with truly inf cladding. As mentioned in Sec. 1, some of us had suggested on the basis of numerical extrapolation techniques, tha fundamental mode of MOFs could be cut off at long wavelengths, which the present, more accurate, study contrac As is evident from Fig. 9, the fundamental mode of solid core MOFs is localized around the core at short wavelen but expands very rapidly into the cladding with increasing wavelength. This behavior is essentially the same as th the fundamental mode of standard step index fibers. However, in the case of MOFs with finite cladding, the fundar tal mode does get cutoff at finite wavelengths. Furthermore, the cutoff wavelength scales as the square root of the l rithm of the cladding size [20], a pathological form of variation which invalidates the numerical extrapolation t niques applied in [2]. This however, does not invalidate our previous conclusions on the wavelength ranges in wh MOFs can be operated remain unchanged. Indeed, recent experimental work has demonstrated the reality of the fu mental mode cutoff in MOFs, with excellent quantitative agreement with our previous predictions [21].

In conclusion, we have presented the FSS that can be used to calculate the modes in infinite periodic structures wi localized defect. The method relies on three conceptual steps: the use of virtual sources, Brillouin zone integration, the use of scattering matrices $\mathbf{R}_\infty$ for a semi-infinite periodic structure, to reduce this integration to a line integral. note that a technique involving virtual scatterers for in-plane propagation was recently reported by Ludwig and Le than [22]. The key difference with our method is that we use a fictitious compound source at the centre of the scatter while Ludwig and Leviathan use sets of dipole sources placed near the boundaries of the scatterers. Our method can applied to both in-plane and out-of-plane propagation, corresponding typically to 2-dimensional photonic crystals a MOFs respectively. Here, however, we have applied it to the latter geometry in which we studied the long-wavelen behavior of the fundamental mode. The FSS method is particularly well-suited for this problem since the mode fi becomes extremely large in this limit.

ACKOWLEDGEMENTS

The authors are grateful for interesting and useful discussions regarding this work with Dr Chris Poulton and with Pr Philip Russell and Jonathan Knight. This work was produced with the assistance of the Australian Research Coun under the ARC Centres of Excellence Program.

REFERENCES

1 T. A. Birks, J. C. Knight, and P. St.J. Russell, "Endlessly single-mode photonic crystal fiber," Opt. Lett. **22**, 96 963 (1997).

2 B. T. Kuhlmey, R. C. McPhedran, C. M. de Sterke, P.A. Robinson, G. Renversez, and D. Maystre, "Microstructured optical fibers: where is the edge?", Optics Express **10**, 1285-1291 (2002). http://www.opticsexpress.org/abstract.cfm?URI=OPEX-10-22-1285.

3 B. T. Kuhlmey, R. C. McPhedran, and C. M. de Sterke, "Modal 'cutoff' in microstructured optical fibers," Optics Letters **27**, 1684-1686 (2002).

4 S. Wilcox, L. C. Botten, R. C. McPhedran, C. G. Poulton and C. M. de Sterke, "Exact modelling of defect modes in photonic crystals using the fictitious source superposition method," Phys. Rev. E **71**, 056606 (2005).

5 L. C. Botten, R. C. McPhedran, C. M. de Sterke *et al*, "From multipole methods to photonic crystal device modelling," Chapter 2 in *Electromagnetic Theory and Applications for Photonic Crystals*, edited by K. Yasumoto, CRC Taylor and Francis (2005), in press.

6 L. C. Botten, N. A. Nicorovici, A. A. Asatryan, R. C. McPhedran, C. M. de Sterke, and P. A. Robinson, "Electromagnetic scattering and propagation through grating stacks of metallic and dielectric cylinders for photonic crystal calculation. Part 1: Formulation," J. Opt. Soc. Am. A **17**, 2165–2176 (2000).

7 L. C. Botten, N. A. Nicorovici, R. C. McPhedran, A. A. Asatryan, and C. M. de Sterke, "Photonic band structure calculations using scattering matrices", Phys. Rev. E **64**, 046603 1-20 (2001).

8 L. C. Botten, T. P. White, A. A. Asatryan, T. N. Langtry, C. M. de Sterke and R. C. McPhedran, "Bloch mode scattering matrix methods for modelling extended photonic crystal structures. Part I: Theory", Phys. Rev. E **70**, 056606 (2004).

9 L. C. Botten, A. A. Asatryan, T. N. Langtry, T. P. White, C. M. de Sterke, and R. C. McPhedran, "Semi-analytic treatment for propagation in finite photonic crystal waveguides", Optics Letters **28**, 854-856 (2003).

10 T. P. White, L. C. Botten, R. C. McPhedran, and C. M. de Sterke, "Ultra-compact resonant filters in photonic crystals", Optics Letters **28**, 2452-2454 (2003).

11 T. P. White, C. M. de Sterke, R. C. McPhedran, T. Huang, and L. C. Botten, "Recirculation-enhanced switching in photonic crystal Mach-Zehnder interferometers", Opt. Express **12**, 3035-3045 (2004).

12 T. P. White, B. T. Kuhlmey, R. C. McPhedran, D. Maystre, G. Renversez, C. M. de Sterke, and L. C. Botten, "Multipole method for microstructured optical fibers I: Formulation", J. Opt. Soc. Am. A **19**, 2322-2330 (2002).

13 B. T. Kuhlmey, T. P. White, G. Renversez, D. Maystre, L. C. Botten, C. M. de Sterke, and R. C. McPhedran, "Multipole method for microstructured optical fibers II: Implementation and Results", J. Opt. Soc. Am. A **19**, 2331-2342, (2002).

14 B. T. Kuhlmey, computer code, CUDOS MOF Utilities, available at http://www.physics.usyd.edu.au/cudos/mofsoftware/index.html.

15 A. Bjarklev, J. Broeng, and A.S. Bjarklev, *Photonic crystal fibers* (Kluwer, Boston, 2003).

16 S. Wilcox, L. C. Botten, C. M. de Sterke, B. T. Kuhlmey, R. C. McPhedran, D. P. Fussell, S. Tomljenovic-Hanic, "Long wavelength behaviour of the fundamental mode in microstructured optical fibers," Optics Express **13**, 1978-1984 (2005). http://www.opticsexpress.org/abstract.cfm?URI=OPEX-13-6-1978

17 M. Yan and P. Shum, "Antiguiding in microstructured optical fibers," Opt. Express **12**, 104-116 (2004), http://www.opticsexpress.org/abstract.cfm?URI=OPEX-12-1-104.

18 M. Koshiba and K. Saitoh, "Applicability of classical optical fiber theories to holey fibers," Opt. Lett. **29**, 1739-1741 (2004).

19 A.W. Snyder and J.D. Love, *Optical waveguide theory* (Chapman and Hall, London, 1983).

20 R. J. Black and R. Bourbonnais, "Core-mode cutoff for finite cladding lightguides," IEE Proc. J **133**, 377-384 (1986).

21 H. C. Nguyen, B. T. Kuhlmey, M. J. Steel, C. L. Smith, E. C. Mägi, R. C. McPhedran and B. J. Eggleton, "Leakage of the fundamental mode in photonic crystal fiber tapers," Opt. Lett. **30**, 1123-1125 (2005).

22 A. Ludwig and Y. Leviathan, "Analysis of arbitrary defects in photonic crystals by use of the source model technique," J. Opt. Soc. Am. A **21**, 1334-1343 (2004).